J. Ind. Geophys. Union (November 2016)
v.20, no.6, pp: 536-543

Imaging of seismic discontinuities of the upper mantle in the western Himalaya through Receiver Function analysis

Nagaraju Kanna*, K.S. Prakasam, Sandeep Gupta, K. Sivaram, Sudesh Kumar, Somasish Bose and B.N.V. Prasad

CSIR-National Geophysical Research Institute, Uppal Road, Hyderabad-500007, India
*Corresponding Author: nagarajugeo@gmail.com

ABSTRACT

We present image of seismic velocity discontinuities of the upper mantle in the depth range of 200 to 800 km beneath the western Himalaya from Gangetic Plain (27.5ºN latitude) to Ladakh-Karakoram region (35ºN latitude), an active collision zone of Indo-Eurasian plates. We use 2088 Receiver Functions calculated from the data obtained from 44 digital broadband seismological stations. The results show a sharp 410 km discontinuity in the range of ~393 – 406 km from Gangetic Plain till Indus Zangpo Suture (IZS), and disturbed (double peaked) further north of the IZS. The 660 km discontinuity shows flat and sharp discontinuity in the Gangetic Plain through Himalaya and elevated ~12 to 17 km beneath Tibetan Himalaya to the north of IZS. We observe a distinct northward dipping velocity interface to the north of IZS in the depth range of ~460 to 490 km which indicates down going Indian subducting slab reported in earlier studies. This velocity interface may be responsible for earlier 660 km phase beneath this region. Thickened mantle transition zone (~255-262 km) is observed beneath Gangetic Plain and NW Himalaya than Tibetan Himalaya due to presence of cold material within (~100º C less than normal).

Key words: Receiver Function, Common Depth Point Stacking, 410 and 660 global discontinuities, Mantle Transition Zone and Western Himalaya.

INTRODUCTION

Deep imaging of Indo-Eurasian Plates collision zone is essential to understand the evolution of the Himalaya-Tibetan belt. Majority of the previous studies reveal that the Himalaya-Tibetan belt is evolved mainly by underthrusting of the Indian crust with mantle lithosphere (e.g., Argand, 1924; Ni and Barazangi, 1984; Mattayer, 1986; Oreshin et al., 2008). Two different hypotheses exist about the nature of the collision zone. Argand (1924) proposed a flat underthrusting of Indian plate beneath Eurasian plate and later supported by many others (e.g., Ni and Barazangi, 1984; Zhou and Murphy, 2005). Another one suggests that the Indian plate, with its crust scraped off plunges steeply into the asthenosphere (e.g., Mattayer, 1986; Replumaz et al., 2004). Many seismic experiments have been carried out in the Himalaya-Tibetan belt to understand the nature of crust and upper mantle (e.g., Molnar, 1988; Hirn et al., 1995, Van der Voo et al., 1999; Zhao et al., 2001; Kind et al., 2002; Ritzwoller et al., 2002; Tilman et al., 2003; Replumaz et al., 2004; Wittliger et al., 2004; Schulte-Pelkum et al., 2005; Kumar et al., 2006; Li et al., 2006; Priestley et al., 2006; Rai et al., 2006; Oreshin et al., 2008; Caldwell et al., 2009; Nábělek et al., 2009; Zhang et al., 2012; Devi et al., 2011; Caldwell et al., 2013). Most of these studies are carried out using the data from Tibetan side and revealed the nature of collision zone is not unique from east to west along the Himalaya-Tibetan belt and different in different parts of the Himalaya-Tibetan collision zone. This non-uniqueness might arise from insufficient resolution of the data or complexity of the actual deep structure. However, the internal structure of the upper mantle of Indian plate still is not well understood due to data paucity from Indian side.

Several investigations have been carried out to understand nature of upper mantle using seismic discontinuities at 410 and 660 km which are most significant and best observed seismic reflectors in the mantle and associated with phase transformations within the olivine dominated peridotite system (Agee, 1993), leading to an increase in compressional and shear wave velocities across them. The 410 km discontinuity marks the transformation from olivine to α- spinel, and the 660 km discontinuity marks the transformation from β- spinel to perovskite + magnesiowüstite (Kind et al., 2002). Both the reactions are sensitive to the temperature and have Clapeyron slopes of opposite signs. The zone between these two discontinuities is called Mantle Transition Zone (MTZ). The thickness of the MTZ provides direct information about temperature within it and adjacent part of the mantle and thus constitutes an important constraint on geodynamic and geochemical models for mantle processes. The expected magnitude of the effect is about ~100º C per ~10 km thickness change of the transition zone (Kind et al., 2002). Thickened mantle transition zone is found in subduction and colder region and thinner mantle transition zone is found in oceanic plates, the region having mantle plumes and warmer region. The structure

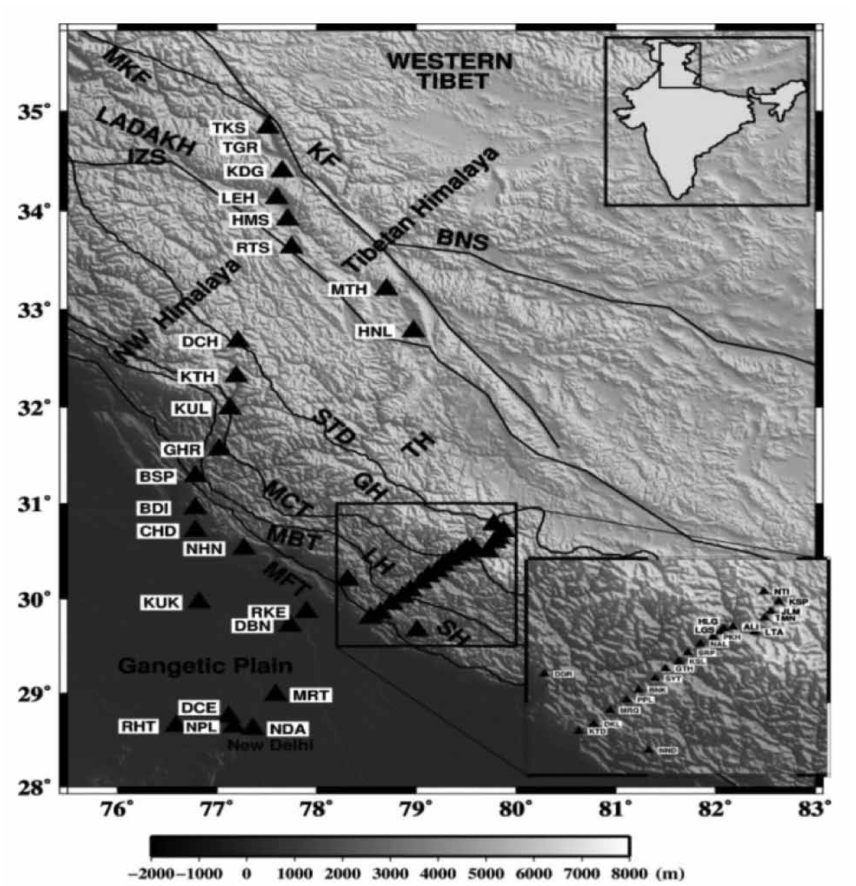

Figure 1. The tectonic map, projected over topography of the study region showing subdivisions of Gangetic Plain, NW Himalaya and Ladakh by the major thrusts with solid continuous lines from south: MFT- Main Frontal Thrust, MBT- Main Boundary Thrust, MCT- Main Central Thrust, STD- Southern Tibet Detachment, IZS- Indus Zangpo Suture, KF- Karakoram Fault, MKF- Main Karakoram Fault, BS- Bangang Nuziang Suture, SH- Sub Himalaya, LH- Lesser Himalaya, GH- Greater Himalaya, TH-Tethys Himalaya. The triangles represent the seismic stations used in this study.

of mantle transition zone provides good constraint to understand the evolution of the Himalaya-Tibetan belt.

Earlier study of mantle transition zone by Wittlinger et al., (2004) reported ~10 km elevated 410 km discontinuity beneath the southern part of western Tibet due to the presence of colder material (~100° C less temperature), whereas, Kind et al., (2002) reported late arrival of 410 and 660 discontinuities beneath central Tibet due to presence of hotter material (more than ~300° C temperature).

A study of MTZ for whole of India, from southern tip of India to Karakoram, was carried out by Rai et al., (2009) using 1957 Receiver Functions of Gaussian width 0.6 from 54 broadband seismographs operated during 1999-2004 with depth interval of 5 km using the Receiver Functions and presented a ~10 km thickened mantle transition zone in the Gangetic Plain than India. The number of stations was limited to 16 for the Himalayan region. Singh et al., (2015) present the review of the crust and upper mantle structure from the Indian subcontinent to Himalaya. With large data available for the Western Himalaya from the seismic stations operated during 2005-2008 and 2011-2012, we study the western Himalaya region in more detail.

Geological Settings

The long ~2400 km Himalaya-Tibetan belt is formed by underthrusting of the Indian plate that continues to push the Eurasian plate since ~50 Ma (Patriat and Achache, 1984). During this process, several fault systems have been created from south to north, as: Main Frontal Thrust (MFT), Main Boundary Thrust (MBT), Main Central Thrust (MCT), South Tibetan Detachment (STD), Indus Zangpo Suture(IZS), Main Karakoram Fault (MKF), Karakoram Fault (KF), and Bangong Nuziang Suture (BS). The present study area is the western extremity of the Himalaya –Tibet orogen and comprises of three major structural blocks, the Tibetan Himalaya and NW Himalaya separated by the Southern IZS and the Gangetic Plain to the south of MFT. The Tibetan block consists of Ladakh and Karakoram to the north of IZS. To the south of IZS lies the Tethys Himalaya with the STD as the southern boundary. To the south of the STD lies the Himalayan sequence, consisting of the Higher (or Greater) Himalaya, Lesser (or Lower) Himalaya and Sub (or Outer) Himalaya, which are bounded between the STD - MCT, MCT – MBT and MBT – MFT thrust zones, respectively. Figure 1 shows the study region and major geological boundaries with the topography of the region. Its evolution and internal structure has been subject of numerous geological and geophysical studies (e.g., Molnar, 1988; Klemperer, 2006).

Data

In the present study, we use data of 44 broadband seismological stations deployed in the western Himalaya in different periods. Out of 44 stations, 15 stations are operated during 2002 to 2003 in the NW Himalaya and Ladakh (Rai et al., 2006), 10 stations are operated during 2005 to 2008 in the Gangetic Plain (Borah et al., 2015) and remaining 19 stations are operated during 2005 to 2008 and 2011 to 2012 in the Kumaon-Garhwal Himalaya (Mahesh et al., 2013). The stations locations are shown in Figure 1.

Each station consists of a Guralp CMG-3T or 3ESP sensor with time tagging using Global Position System (GPS) and a refraction technology data logger continuously recording waveforms at 20 samples per second for the stations in the NW Himalaya and Ladakh and 50 samples per second for the other stations. For consistency, the waveforms are decimated to 20 samples per second. Earlier this data set is used to map the Moho discontinuity of the study region (Rai et al., 2006; Caldwell et al., 2013; Oreshin et al., 2008). The inferred Moho depth varies from ~40 to 75 km from the Delhi region to Ladakh in the Tibetan Himalaya.

METHODOLOGY

We use the well known seismological technique of the Receiver Function to map the seismic discontinuities in the upper mantle. This technique utilizes the waves converted (P to S) at velocity discontinuities to study the nature of the Earth's structure directly beneath the receiver. The arrival time and amplitude of the converted phase provide us the information related to depth location, width and possible causal mechanisms of the discontinuity. We select good teleseismic earthquakes having high signal to noise ratio (S/N) with magnitude greater than 5.5 and within the distance range of 30 to 90^{o}. Further, we calculate the Receiver Functions at each station using time domain deconvolution method of Ligoria and Ammon (1999). Since our interest is to map the discontinuities in the deep depth in the upper mantle (200 to 800 km), we filter the waveforms in a low frequency band with a Gaussian width of 1.0 corresponding to a frequency of less than 0.5 Hz. The depth resolution for Receiver Function at Gaussian width factor of 1.0 is ~1.9 km (Sheriff and Geldart, 1995). We carefully examine the Receiver Functions at each station and finally select 2088 Receiver functions with good Signal to Noise ratio for our analysis.

We use "Common Depth Point" (CDP) stacking technique of Dueker and Sheehan (1997) to map the 3-D structure of the upper mantle. The following steps are involved in the CDP stacking approach,

i. Computation of geographical locations of the piercing points of all P to S conversions for each source-receiver pair at 2 km depth increments from 200 to 800 km, using TauP toolkit (Crotwell et al., 1999) with respect to a reference model. The crustal part of this reference model is obtained from the Receiver Function modeling of each station (unpublished data) and further deep in the model, we add the IASP91 velocity model (Kennet and Engdahl, 1991).

ii. Calculation of the travel times of P to S converted phase (T_{pds}) from various depths using the formula,

$$T_{pds} = \int_{-d}^{0} \left(\sqrt{V_S(z)^{-2} - p^2} - \sqrt{V_P(z)^{-2} - p^2}\right) dz \qquad (1)$$

Where p is the rayparameter for P wave, d represents the depth of the discontinuity and $V_P(z)$ and $V_S(z)$ are the P and S wave velocities at depth z.

iii. Dividing the study area into rectangular blocks of fixed width as 0.5^{o} in latitude and varying length 4-6^{o} in longitude depending on their piercing points at each depth. Piercing point is the location at depth, where the P-to-S conversion occurs. To produce the depth image of discontinuity, the amplitudes from individual receiver functions piercing a particular area are summed (stacked) using:

$$A(d) = \frac{1}{N}\sum_{i=1}^{N} A_i(T_{pds}) \qquad (2)$$

Where A(d) is the stacking amplitude for a candidate discontinuity at depth d, N is the number of receiver function piercing particular depth d.T_{pds} is the Pds move out time of the corresponding receiver function for a discontinuity computed using the equation (1). $A_i(T_{pds})$ is amplitude of the i^{th} receiver function.

We use bootstrap resampling technique (Efron and Tibshirani, 1986) to ascertain the uncertainties that results from variation and/or noise in the Receiver Functions. We select 95% of the piercing points in rectangle box and run the 50 iterations of the CDP stack with group of the points randomly selected from the full pool (with duplication, so that the number of points for each iteration is same as the number of unique points). The mean depth of discontinuity

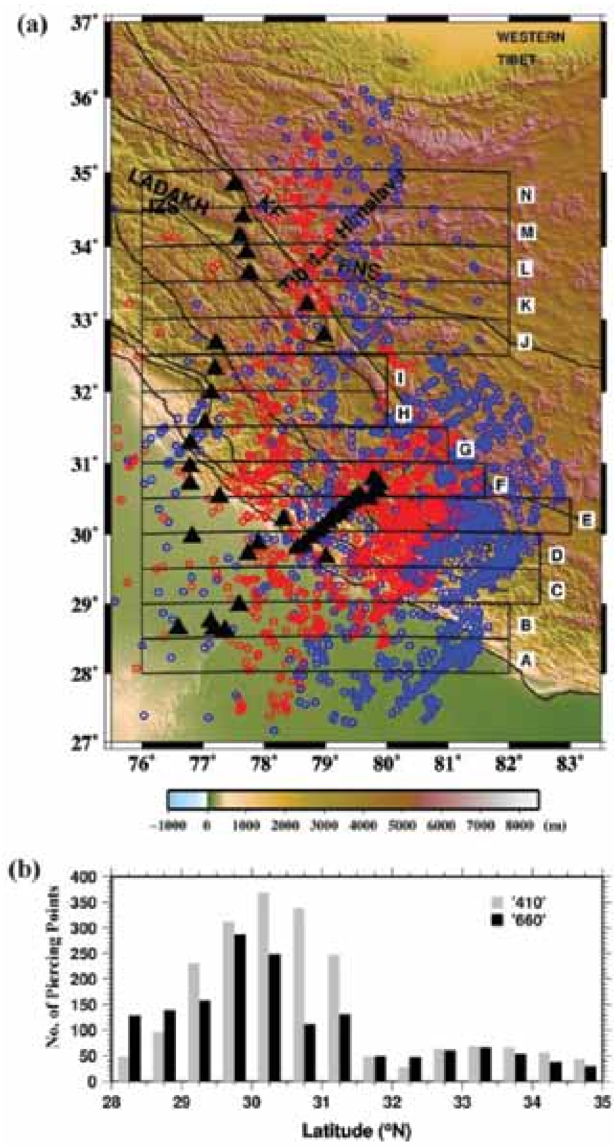

Figure 2. (a) Distribution of piercing points of P to S converted phases at 410 (red circles) and 660 km (blue circles) depth. Triangles represent seismic stations. Rectangular boxes (A to N) show the node for which Receiver Functions are stacked and present as its mid-point. The geological structures are same as Figure 1. (b) Number of piercing points of 410 (gray color) and 660 (black) km discontinuities used for each block.

on each rectangle box from those iterations is calculated using the following formula,

$$\bar{D} = \frac{1}{N}\sum_{i=1}^{N} D_i \tag{3}$$

where N is the number of bootstrap, D_i is the depth of the 410 and 660 km discontinuities corresponding toe maximum stacking amplitude in the depth ranges of 410±25 and 660±25 km from the i^{th} bootstrap. Standard deviation of the mean depths, σ_{410} and σ_{660} are calculated using:

$$\sigma_d = \frac{1}{N-1}\sum_{i=1}^{N} (D_i - \bar{D})^2 \tag{4}$$

where d is the 410 or 660 km discontinuity. Further, the mantle transition zone thickness is estimated by depth differences of the 660 km and the 410 km discontinuity in the rectangular block. The standard deviation for the mantle transition zone (MTZ) thickness is:

$$\sigma_{MTZ} = \sqrt{\sigma_{410}^2 + \sigma_{660}^2} \tag{5}$$

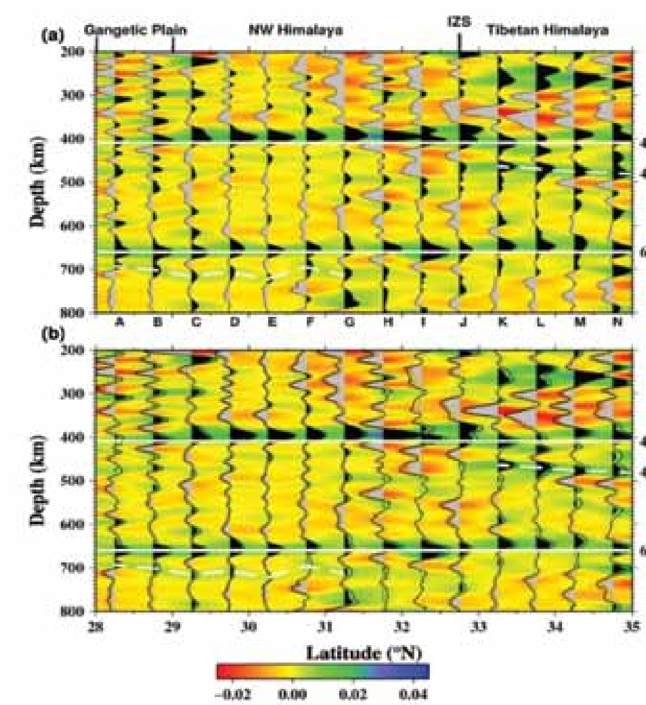

Figure 3. The stacked Receiver Functions from the Gangetic Plain to Ladakh-Karakoram i.e in the Tibetan Himalaya without bootstrap technique (a) and with bootstrap resampling (b). The color scale indicates size of the amplitude.

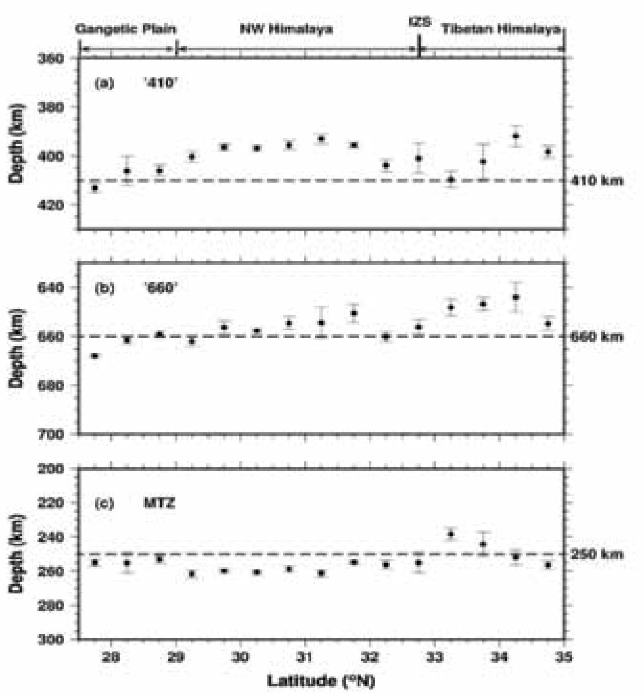

Figure 4. Depth of (a) 410 km discontinuity, (b) 660 km discontinuity and (c) thickness of the mantle transition zone calculated at each block shown in Figure 2.

RESULTS AND DISCUSSION

The geographical distribution of piercing points at P410s km (red circles) and P660s km (blue circles) are illustrated in Figure 2a and the number of points in each rectangular block corresponding to mean latitude is shown in Figure 2b. We reduce the length of four blocks (F to I), to the south of the Indus Zangpo Suture, to avoid the piercing points at P660s falling in Tibetan Himalaya (see Figure 2b).We have fairly large number of piercing points in the NW Himalaya region and moderately good number of points for the Tibetan Himalaya region. Figure 3 shows the stacked Receiver Functions with depth, without bootstrap procedure (Figure 3a) and with bootstrap procedure (Figure 3b) at each sampled block of 0.5^{o} in latitude. In both the cases the main features are comparable. Figure 3b shows the smooth image and we use it for further discussion/ interpretation. The variation of representative depths of 410 and 660 discontinuities and the thickness of mantle transition zone are shown in Figure 4 with error bars.

410 km Discontinuity

In the Gangetic Plain the 410 discontinuity is observed at ~406 km being gradually uplifted to ~393 km in the NW Himalaya and reaches to ~402 km to the south of Indus Zangpo Suture (Figure 4a). However, it shows complex nature (nearly double peak for I, J, L, M and N; Figure 3b) at Indus Zangpo Suture and further north where it reaches to ~392-400 km in Ladakh, i.e Tibetan Himalaya. This complex signature is observed in the data without bootstrap as well (Figure 3a) therefore, we assume that the 410 discontinuity is of complex nature beneath this region. Similar observation is reported by Wittlinger et al., (2004) in the southern part of western Tibet to the north of our study region. The observed systematic elevation of the 410 discontinuity beneath the NW Himalaya may be the presence of thickened high velocity layer at shallow mantle in this region, reported in the earlier studies (e.g., Ritzwoller et al., 2002; Priestley et al., 2006; Oreshin et al., 2008). However this discontinuity appears slightly deeper beneath northern Tibet and with possible presence of hotter material in the upper mantle (Kind et al., 2002; Wittlinger et al., 2004).

475 km Discontinuity

A significant sharp northward dipping high velocity interface in the depth range of 460-490 km is observed to the north of Indus Zangpo Suture (Figure 3b), beneath the Tibetan Himalaya, which is not observed beneath Gangetic plains and Himalaya. In the Himalaya-Tibetan belt, the crustal thickness varies between 70 and 80 km (Rai et al., 2006). The multiples with respect to the Moho conversion (around 8 – 10 s) can be observed around 25 to 30 s, which generally corresponds to ~250-300 km depth. The presence of multiples in the depth range of 460 to 490 km (i.e., 46 – 49 s) requires a strong conversion in the Receiver Functions in the time range of ~13 to 17 s. Although, we observe some peaks in this time range, however these peaks are weak, rather than strong amplitudes, and thus can be the multiples of mid-crustal conversions (~4.5 to 6 s) present in this complex Himalaya-Tibet region. Further, this depth range is shallower than ~520 km global discontinuity. Since this depth range is shallower than the 520 km global discontinuity and greater than shallower multiples of shallow depth conversions, it may be interpreted as relic of the subducted oceanic slab as observed in the tomographic images (Ritzwoller et al., 2002; Priestley et al., 2006) and the sinking slab may be responsible for the disturbed 410 km discontinuity present in this region. Similar observation was reported by Rai et al., (2009) in the Ladakh-Karakoram region and Wittlinger et al., (2004) in the southern part of western Tibet, whereas it is not seen in the central Tibet (Kind et al., 2002).

660 km Discontinuity

We observe a sharp 660 km discontinuity throughout the study region (Figure 3b) instead of complex 660 km discontinuity as reported by Rai et al., (2009). The depth of this discontinuity beneath Gangetic Plain is observed around ~660 km, whereas, it varies from ~650 to 662 km beneath the NW Himalaya and elevated to ~644 to 654 km in the Tibetan Himalaya, to the north of Indus Zangpo Suture (Figure 4b). The uplift of 660 km in the Tibetan Himalaya may be possibly due to the presence high velocity ~475 km discontinuity. A weak positive discontinuity at a depth of 670-700 km is observed from Gangetic plan to Indus Zangpo Suture but the consistency is missing in the Tibetan Himalaya (Figure 3b). The discontinuity at 655-661 km is a result of phase change from garnet to ilmenite and the discontinuity at 670-700 km could be the result of transformation from ilmenite to pervoskite (Rai et al., 2009).

Mantle Transition Zone

Our results show that the mantle transition zone thickness is at ~254 km for the Gangetic Plain, whereas it varies in the range of ~255 to 262 km beneath the NW Himalaya (Figure 4c). It decreases to ~239-244 km immediately to the north of Indus Zangpo Suture and increases to 251-256 km further north beneath the Tibetan Himalaya (Figure 4c). We observe the mantle transition zone thickness is more beneath the Gangetic Plain and NW Himalaya than the Tibetan Himalaya. The thickened mantle transition zone in Gangetic plan and Himalaya is suggestive of presence of colder material than the Tibetan Himalaya. Also similar observation is presented using travel time residuals by Oreshin et al., (2008). Rai et al., (2009) also reported ~10 km more thickened mantle transition zone in the Gangetic Plain compared to India.

CONCLUSIONS

In the present study, we map the mantle transition zone of the western Himalaya. These values are comparable with the earlier results of mantle transition zone study of the Indian subcontinent, from Kanyakumari to Karakoram (Rai et al., 2009). They used 1957 receiver functions with Gaussian width 0.6 and stacked at bin latitude of 1.0^{o} which facilitated a smooth picture of the study region. We adopted the same methodology of Rai et al., (2009) using 2088 Receiver Functions of Gaussian width 1.0 with a stacked bin of 0.5^{o} latitude, thus obtaining reasonably constrained values. Our results show a sharp and gradually elevated 410 discontinuity from Gangetic Plain to the NW Himalaya upto the Indus Zangpo Suture, further complex in the Tibetan Himalaya. We also observed a sharp 660 km discontinuity in the entire study region and uplifted in the Tibetan Himalaya. The elevated 410 km discontinuity may be underthrusting of the Indian lithosphere slab in the shallower mantle (upto a depth of 300 km) as seen in the tomographic images in the study region. The observed northward dipping high velocity interface at ~475 km may be the signature of broken Tethys slab and may be responsible for the complex (double peak) 410 and elevated 660 km discontinuities in the Tibetan Himalaya (Rai et al., 2009). The thickened mantle transition zone in the NW Himalaya by about ~12 km than Tibetan Himalaya indicates a colder NW Himalaya by about ~100 C (Oreshin et al., 2008). A weak positive discontinuity at a depth range of 670-700 km is observed from Ganges basin to NW Himalaya but the consistency is missing further in the Tibetan Himalaya.

ACKNOWLEDGEMENTS

The field program was supported by Department of Science & Technology, Govt. of India. We are very thankful to the members of Seismic Tomography group of CSIR-NGRI, for their support during seismological stations deployment. NK is supported by research fellowship from the Ministry of Social and Justice Empowerment, Govt. of India. Figures are made with Generic Mapping Tools. Support from CSIR Research projects MLP-6505-28(SKG) and INDEX-0204 are acknowledged. Authors are also thankful to Prof. B.V.S. Murthy and Chief Editor for useful suggestions and appropriate editing of the manuscript.

Compliance with ethical standards

The authors declare that they have no conflict of interest and adhere to copyright norms.

REFERENCES

Agee, C., 1993. Petrology of the mantle transition zone, Ann. Rev. Earth Planet. Sci., v.21, pp: 19-41.

Argand, E., 1924. La tectonique de I'Asie, Int. Geol. Cong. Resp. Sess., v.13, pp: 170-372.

Borah, K., Nagaraju, K., Rai, S.S., and Prakasam, K.S., 2015. Sediment thickness beneath the Indo-Gangetic Plain and Siwalik Himalaya inferred from Receiver Function, J. Asian Earth Sci., v.99, pp: 41-56.

Caldwell, W.B., Klemperer, S.L., Rai, S.S., and Lawrence, J.F., 2009. Partial melt in the upper-middle crust of the northwest Himalaya revealed by Rayleigh wave dispersion, Tectonophysics, v.477, pp: 58-65.

Caldwell, W.B., Klemperer, S.L., Lawrence, J.F., Rai, S.S., and Ashish, 2013. Characterizing the Main Himalayan Thrust in the Garhwal Himalaya, India with receiver function CCP stacking, Earth Planet. Sci. Lett., v.367, pp: 15-27.

Crotwell, H.P., Owens, T.J., and Ritsema, J., 1999. The TauP Toolkit: Flexible seismic travel time and raypath utilities, Seismol. Res. Lett., v.70, pp: 154-170.

Devi, E.U., Kumar, P., and Kumar, M.R., 2011. Imaging the Indian lithosphere beneath the eastern Himalayan region, Geophys. J. Int., v.187, pp: 631-641.

Dueker, K.G., and Sheehan, A.F., 1997. Mantle discontinuity structure from midpoint stacks of converted P to S waves across the Yellowstone hotspot track, J. Geophys. Res., v.102, pp: 8313-8327.

Efron, B., and Tibshirani, R., 1986. Statistical data analysis in the computer age, Sci., v.253, pp: 390-395.

Hirn, A., Jiang, M., Sapin, M., Diaz, J., Nercessian, A., Lu, Q.T., Lepine, J.C., Shi, D.N., Sachpazi, M., Pandey, M.R., Ma, K., and Gallart, J., 1995. Seismic anisotropy as an indicator of mantle flow beneath the Himalayas and Tibet, Nature, v.375, pp: 571-574.

Kennet, B., and Engdahl, E., 1991. Travel times for global earth location and phase identification,Geophys. J. int., v.105, pp: 429-465.

Kind, R., Yaun, X., Saul, J., Nelson, D., Sobolev, S.V., Mechie, J., Zhao, W., Kosarev, G., Ni, J., Achauer, U., and Jiang, M., 2002. Seismic images of crust and upper mantle beneath Tibet: evidence for Eurasian plate subduction, Sci., v.298, pp: 1219-1221.

Klemperer, S.L., 2006. Crustal flow in Tibet: geophysical evidence for the physical state of Tibetan lithosphere and inferred patterns of active flow, in channel Flow, Ductile Extrusion and Exhumation in Continental Collision Zones, Geol. Soc. Lond. special publications, v.268, pp: 39-70.

Kumar, P., Yuan, X., Kind, R., and Ni, J., 2006.Imaging the colliding India and Asian lithospheric plates beneath Tibet, J. Geophys. Res.,doi: 10.1111/j.1365-246x.2008.03777x., v.111.

Li, Q., Van Der Hilst, R.D., and Toksoz, M.N., 2006. Constraining P velocity variations in the upper mantle beneath Southeast Asia, Phys. Earth Planet. Inter., v.154, pp: 180-195.

Ligorria, J.P., and Ammon, C., 1999. Iterative deconvolution and receiver-function estimation, Bull. Seismol. Soc. Am., v.89, pp: 1395-1400.

Mahesh, P., Rai, S.S., Sivaram, K., Ajay, P., Sandeep, G., Sarma, P.R., and Gaur, V.K., 2013. One-Dimensional reference velocity model and precise locations of earthquake Hypocenters in the Kumaon-Garhwal Himalaya, Bull. Seismol. Soc. Am., v.103, pp: 328-339.

Mattayer, M., 1986. Intracontinental subduction, crust-mantle decollement and crustal stacking wedge in the Himalayas and other collisional belts, In: Coward, M.P., Ries, A.C. (Eds.), Collision Tectonics, Geol. Soc. Lond. Spec. Pub., v.19, pp: 37-50.

Molnar, P., 1988. A review of geophysical constraints on the deep structure of the Tibetan Plateau, the Himalaya and the Karakoram and their tectonic implications,Phil. Trans. R. Soc. Lond. Ser., v.326, pp: 33-88.

Nábělek, J., Hetenyi, G., Vergne, J., Sapkota, S., Kafle, B., Jiang, M., Su, H., Chen, J., Huang, B., and the Hi-CLIMB Team, 2009. Underplating in the Himalaya-Tibet collision zone revealed by the Hi-CLIMB experiment, Sci., v.325, pp: 1371-1374.

Ni, J., and Barazangi, M., 1984. Seismotectonics of the Himalayan collison zone: geometry of the underthrusting Indian plate beneath the Himalaya, J. Geophys. Res., v.89, pp: 1147-1163.

Oreshin, S.S., Kiiselev, S., Vinnik, L., Prakasam, K.S., Rai, S.S., Makeyeva, L., and Savvin, Y., 2008. Crust and mantle beneath western Himalaya, Ladakh and western Tibet from integrated seismic data, Earth Planet, Sci. Lett., v.271, pp: 75-87.

Patriat, P., and Achache, J., 1984. India–Asia collision chronology has implications for crustal shortening and driving mechanism of plates, Nature, v.311, pp:615–621.

Priestley, K., Dabayle, E., McKenzie, D., and Pilidou, S., 2006. Upper mantle structure of eastern Asia from multimode surface waveform tomography, J. Geophys. Res.,doi:10.1029/2005JB004082., v.111.

Rai, S.S., Priestley, K., Gaur, V.K., Mitra, S., Singh, M.P., and Searle, M.P., 2006. Configuration of the Indian Moho beneath the NW Himalaya and Ladakh, Geophys. Res. Lett.,doi: 10.1029/2006GL026076., v.33.

Rai, S.S., Prakasam, K.S., and Gaur, V.K., 2009. Seismic imaging of the mantle discontinuities beneath India: from Archean cratons to Himalayan subduction zone, in Gupta, A., Dasgupta, S. (Eds.), Physics and chemistry of the Earth Interior, Springer New York, pp: 153-161.

Replumaz, A., Karson, H., Var Dar Hilts, R.D., Besse, J., and Tapponier, P., 2004. 4-D evolution of SE Asia's mantle from geological reconstruction and seismic tomography, Earth Planet. Sci. Lett.,v.221, pp: 103-115.

Ritzwoller, M.H., Shapiro, N.M., Barmin, M.P., and Levshin, A.L., 2002. Global surface wave diffraction tomography, J. Geophys. Res., doi:10.1029/2002JB001777., v.107.

Schulte-Pelkum, V., Monsalve, G., Sheehan, A., Pandey, M.R., Sapkota, S., Bilham, R., and Wu, F., 2005. Imaging the Indian subcontinent beneath the Himalaya, Nature, v.435, pp: 1222-1225.

Sheriff, R.E., and Geldart, L.P., 1995. Exploration seismology; History, Theory and Data Acquisition, Cambridge University Press, Cambridge, pp: 592+xv.

Singh, A., Singh, C., and Kennet, B.L.N., 2015. A review of crust and upper mantle structure beneath the India subcontinent, Tectonophysics,v.644, pp: 1-21.

Tilman, F., Ni, J., and Team, I.I.S., 2003. Seismic imaging of the Downwelling Indian lithosphere beneath central Tibet, Sci., v.300, pp: 1424-1427.

Van der Voo, R., Spakman, W., and Bijwaard, H., 1999.Tethyan subducted slab under India, Earth Planet. Sci. Lett., v.171, pp: 7-20.

Wittliger, G., Vergne, J., Tapponier, P., Farra, V., Poupinet, G., Jiang, M., Su, H, Herquel, G., and Paul, A., 2004. Teleseismic imaging of subducting lithosphere and Moho offsets beneath western Tibet, Earth Planet. Sci. Lett., v.221, pp: 117-130.

Zhang, H., Zhao, Z., and Xu, Q., 2012. Crustal and upper mantle velocity structure beneath Central Tibet by P-wave teleseismic tomography, Geophys. J. Int., v.190, pp: 1325-1334.

Zhao, W., Mechie, J., Brown, L.D., Guo, J., Haines, S., Heam, T., Kemplerer, S.L., Ma, Y.S., Meissner, R., Nelson, K.D., Ni, J., Pananont, P., Rapine, R., Ross, A., and Saul, J., 2001.Crustal structure of central Tibet as evidence from project INDEPTH wide-angle seismic data, Geophys. J. Int.,v.145, pp: 486-498.

Zhou, H.W., and Murphy, M., 2005. Tomographic evidence for whole scale underthrusting of India beneath the entire Tibetan plateau, J. Asian Earth Sci., v.25, pp: 445-457.